Harmonic system analysis of the algae *Valonia utricularis*: contribution of an electrogenic transport system to gain and phase-shift of the transfer function

Jianning Wang, Günter Wehner, Roland Benz, and Ulrich Zimmermann

Lehrstuhl für Biotechnologie, Biozentrum der Universität Würzburg, D-8700 Würzburg, Germany

ABSTRACT   Cell membrane properties of the giant marine alga *Valonia utricularis* were measured in the frequency domain between 1 Hz and 10 MHz by harmonic system analysis. Harmonic analysis was performed by imposing a sinusoidal electrical voltage on the cell interior via an internal microelectrode. Gain and phase-shift of the resulting sinusoidal membrane voltage were measured over the whole frequency range with an internal voltage microelectrode. Bode plots of gain and phase-shift allowed the determination of the electrical parameters of the equivalent electronic circuits of the cell membrane of *V. utricularis,* which showed dynamic and passive properties dependent on the pH of the external aqueous solution. The dynamic components of the membrane impedance were caused by an electrogenic transport system for chloride described previously (Wang, J., G. Wehner, R. Benz, and U. Zimmermann. 1991. *Biophys. J.* 59:235–248). The kinetic and equilibrium parameters of the transport system could be evaluated from the fit of Bode plots of gain and phase-shift. The frequency domain technique revealed complete agreement of transport parameters with previously published results. The data demonstrate that an electrogenic transport system can be driven by an oscillating electric field.

INTRODUCTION

Electrical properties of cell membranes are important parameters for the maintenance and understanding of cell functions. Passive electrical properties of biological membranes have been measured by many different techniques (e.g., single microelectrode methods, voltage-clamp, patch-clamp, and charge-pulse techniques, and electrorotation [1–3]). These techniques have been used successfully to obtain information about channels and transport systems within the biomembrane. Algal cells of large size (diameter >1 mm) have provided a unique system for the study of electrical properties of plant membranes, in particular when internal microelectrodes have been used for the measurements (4–7). The investigation of the electrical properties of these biological systems has demonstrated the specific advantages, but also the limitations, of the above-mentioned technique.

All these techniques use stationary electric fields for the investigations of membrane transport. Alternatively, oscillating electric fields may be used for the study of membrane transport phenomena since it has been shown that membrane proteins can use energy from an external electric field to drive electrogenic transport (8–10). This means that charges associated with intrinsic membrane proteins respond to alternating electric fields and may undergo dielectric relaxations caused by field-induced conformation changes within the proteins. It has to be noted that a transport system can only absorb energy when the frequency of the alternating current (AC) electric field is in the same frequency range as the corresponding chemical reaction, i.e., the movement of charged groups in the membrane. Otherwise, the energy of the oscillating electric field is either dissipated as heat (when the frequency of the AC field is too high) or the transport system is not affected (when the frequency is too low). Theoretical treatment of multistate membrane transport have shown that AC fields are able to drive the transport systems (9–11).

Recent studies have indeed shown that external AC fields are able to generate ATP synthesis in submitochondrial particles (12) and to stimulate potassium or rubidium transport in red blood cells (13, 14). ATP synthesis has a maximum at a frequency of ~ 10 Hz whereas potassium or rubidium influx in red blood cells is highest at an AC frequency of 1 kHz. Interestingly, only a certain field strength of ~ 2 V/cm is able to stimulate maximum rubidium uptake (14). A similar stimulating effect generated by AC fields has been observed for sodium efflux in red blood cells. However, whereas 1 kHz is sufficient to generate maximum rubidium efflux the frequency has to be as high as 1 MHz to drive maximum sodium efflux (14). More recently, the effect of alternating fields on Na^+,K^+-adenosine triphosphatase (ATPase) has been explained on the basis of a channel-like model (15). This model provides a more straightforward description of the voltage dependence of the transport phenomena.

Therefore additional and complementary information on the electrical properties of membranes can be obtained by the method known as harmonic system analysis. Using this type of measurement, a sinusoidal voltage is applied to an unknown electrical system. The current flowing through the system leads to the generation of a voltage across the cell membrane, which represents the output signal. This signal is also sinusoidal, but has a different amplitude and a certain phase-shift as compared with the input signal. Comparison of the input and output signals over the whole frequency range yields the frequency dependence of the gain (or attenuation) of the input signal and the phase-shift between the output and input signals. These functions are limited by the electrical properties of the membrane barrier, which include passive properties such as membrane capacitance and resistance but also dynamic properties caused by electrogenic transport systems within the membrane. The advantage of harmonic system analysis over the
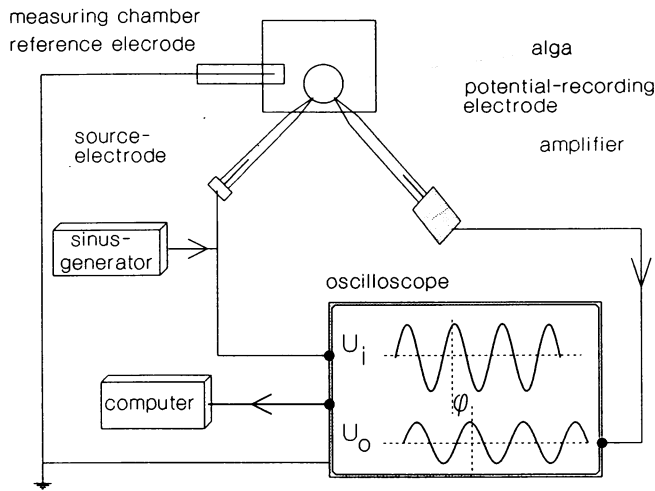
FIGURE 1 Schematic diagram of the setup for the determination of the transfer function of the membrane of *V. utricularis*. For further explanation, see text.

conventional electrical measurements (voltage-clamp, charge-pulse) is its good high-frequency capability.

Harmonic system analysis has been applied widely for automatic control and system theory (16–18). In biology, this method has been used for high-precision interfacial impedance measurements of bioelectrodes (19–22), but not very frequently for the electrical characterization of biomembranes (23–29). We applied harmonic system analysis to the giant marine alga *V. utricularis*. The analysis of the results were consistent with earlier charge-pulse data (30, 31). The presence of the chloride-transport system in the cell membrane (32) leads (in addition to the passive properties of the cell membrane) to characteristic changes of the Bode-plots between 100 Hz and 1 kHz.

MATERIALS AND METHODS

Culture of *V. utricularis*

V. utricularis cells were originally collected in the gulf of Naples, Italy, and were kept in Mediterranean Sea water (MSW) under a 12-h light/dark regime at 17°C. Cells of nearly elliptical shape (volume ~60 mm³, surface area ~100 mm², 11 mo cultivated) were selected for the measurements. During the experiments the cells were immersed either in MSW or else in artificial sea water (ASW) containing 545 mM NaCl, 12 mM KCl, 11 mM $CaCl_2$, and 10 mM $MgCl_2$. If not otherwise stated the pH was adjusted to 8.1 by addition of 10 mM N-2-hydroxyethylpiperazine-N'-2-ethane sulfonic acid/NaOH. For the experiments at pH 4 and 6 MSW was buffered with 10 mM malic acid/NaOH or with 10 mM 2-(N-morpholino) ethane sulfonic acid/NaOH (MES/NaOH), respectively.

Experimental setup

V. utricularis cells were fixed in a plexiglass chamber perfused with MSW or ASW. Two identical and pressure-tight pipette-microelectrodes (outer tip diameter ~30 μm) were positioned in the vacuole of the cell, one for injection of the sinusoidal voltage and the other for potential recording (Fig. 1). The microcapillaries were filled with 3 M

KCl and contained a coiled, 200-μm-thick platinum wire ~1 m in length. The wires had been coated with platinum black (19). The effective surface area of the wires was ~6.3 cm². Thus, polarization of the metal/electrolyte interface could be neglected, which would otherwise lead to a nonlinear electrical behavior of the electrodes (19). To facilitate the interpretation of the frequency spectrum of the cell, matched pairs of microelectrodes were selected for each experiment. The output signal was measured with reference to an external electrode placed in the bulk medium close to the alga surface (a rectangular steel plate, dimensions 28 × 8 mm).

The whole setup was shielded against electromagnetic waves by a Faraday cage. The input sinusoidal signal was generated with a function generator (model TR-0467; EMG, Budapest, Hungary) and the frequency was varied in steps of 1, 1.4, 2, 3, 4, 6, 8, and 10 per frequency decade. Measurements were performed between 1 Hz and 10 MHz. The amplitude of the input signal was ~0.5 V (peak-to-peak value) if not otherwise stated. The output signal was amplified 21-fold by a high-input impedance amplifier based on a wideband fast-settling operational amplifier (model 3554, maximum bandwidth 6 MHz; Burr-Brown Research Corp., Tucson, AZ), which means that the gain was on average 26 dB over the whole frequency range. Since the amplification was frequency independent up to ~6 MHz it was possible to simply subtract the background gain of the amplifier in the Bode plots. The amplifier was connected to the potential-recording electrode by a short cable to minimize noise and cable losses. The input signal and the corresponding amplified output signal were simultaneously monitored with a digital two-channel storage oscilloscope (model 2440; Tektronix, Inc., Beaverton, OR) and stored in an AT-compatible computer (model 2402A, Tektronix). This ensured that the exposure time of the cell to the input voltage for each frequency point could be reduced to ~10 s and that the measurements over the whole frequency range were completed within 5–8 min. To exclude possible (irreversible) changes of the membrane resistance during this period the membrane resistance was measured with a current-clamp (3-μA amplitude and 25-ms duration) before and after the harmonic analysis experiments.

For the harmonic analysis data were processed with an AT-compatible personal computer and custom software was written in-house. After Fourier transformation the gain was calculated from the amplitude ratio of the input and output signals, and the phase-shift by correlation of the two signals. For the fit of the actual data and for the calculation of the parameter of the electronic setup and the membrane barrier, a commercial electronic circuit simulation program (Micro-Cap III; Spectrum Software, Sunnyvale, CA) was used. This program yielded the frequency spectra of gain and of phase-shift of selected electronic circuits in form of Bode plots.

THEORETICAL CONSIDERATIONS

We present here some theoretical aspects of the harmonic analysis, which are needed for the understanding of the analysis of Bode plots. For a more rigorous mathematical treatment the interested reader is referred to the literature (16–18). According to the theory of linear or quasilinear systems the transfer function of a system, $G(s)$, can be calculated:

$$G(s) = Y(s)/X(s). \tag{1}$$

$X(s)$ and $Y(s)$ are the Laplace-transforms of input and output signals, $x(t)$ and $y(t)$, respectively. The transfer function is given in the frequency (Laplace) domain, but not in the time domain. The complex Laplace variable, s, is defined by $s = \delta + i\omega$, where δ is the real and ω is the imaginary part, identical to the angular frequency.

In principle, Eq. 1 is independent of the form of the input signal. However, from a practical standpoint only a few signal forms are useful because: (a) of the accuracy of the measurements and (b) of cell viability (which could be affected by long treatment to an electric field). This means that the signal could be a step function (voltage or current clamp), an impulse (a delta function; charge pulse), or else a sinusoidal function. The use of the latter has the advantage that it allows precise measurements of the transfer function. Furthermore, electromagnetic disturbances and random noise in the output signal can be eliminated easily by averaging and filtering.

The transfer function, $G(s)$, is given for sinusoidal signals by the so-called frequency spectrum, $G(i\omega)$. This complex frequency function can either be separated into a real part, a, and an imaginary part, b, or can be used in the exponential form:

$$G(i\omega) = a + ib = |G(i\omega)| \exp(i\phi). \qquad (2)$$

$|G(i\omega)|$ is the gain, i.e., the ratio of the output to the input amplitude, and ϕ is the phase angle of $G(i\omega)$, i.e., the phase-shift between the output and input signals.

The experimentally determined dependence of gain and phase-shift may be plotted versus the logarithm of the frequency (Bode plots). The phase-shift is given in degrees and the gain in decibels, defined by the following equation:

$$G_{dB} = 20 \log |G(i\omega)| = 20 \log (|Y(i\omega)|/|X(i\omega)|). \qquad (3)$$

Voltage gains of 1, 10, and 100 correspond to 0, 20, and 40 dB, respectively. In the case of the attenuation of the input signal the values become negative since the ratio between output and input signals is always smaller than one. The experimentally determined Bode plots of gain and phase-shift were compared with Bode plots of the equivalent electric circuits. Circuits were selected that yielded identical frequency spectra for both parameters. Once the electric circuit had been determined, it was easy to extract the passive electrical properties of the membrane barrier and the parameters of electrogenic transport systems (if present) from it. It has to be noted that such an approach is not always straightforward because other (either less or more complicated) electronic circuits could be used to fit the same experimental data. The equivalent circuit was chosen that best fitted the prospective electrical characteristics of the biological system (as known from independent measurements) and the components of the measuring device such as electrodes and amplifier (determined in separate experiments without the cell). The experiments described in Results show that the electrical properties of the membrane barrier of V. utricularis are given by circuit A in Fig. 2. This circuit also includes the electrogenic chloride transport in the plasmalemma (see Appendix). The electric circuit B of Fig. 2 (see also reference 24) is equivalent to the circuit A of Fig. 2. The circuit B of Fig. 2 was
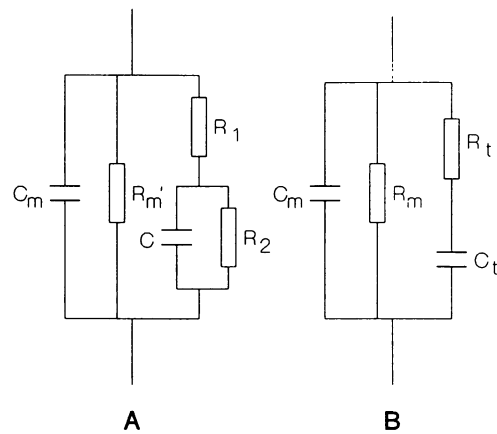

FIGURE 2   Equivalent circuits of the electrical properties of the membrane barrier of V. utricularis (A and B) used in the analysis of the frequency spectra. C_m, specific membrane capacitance; R_m, specific membrane resistance; C, capacitance; R_1 and R_2, resistance of the Cl⁻-transport system. R'_m, specific membrane resistance without the Cl⁻-transport system. Note that circuit B is equivalent to circuit A. The resistance R_t and the capacitance C_t of this circuit have no clearcut physical or biological meaning. This circuit was used for the fitting procedure of the frequency spectra because the mathematical complexity was much reduced. After fitting the curves the electrical parameters of the membrane and the transport system in V. utricularis were calculated by using circuit A.

used (instead of A) to fit the transfer function to the experimental data since it was easier to handle.

RESULTS

Frequency spectra of the measuring device

Interpretation of harmonic analysis of the algal cells was only possible after careful analysis of the spectra due to the measuring device. The input signal was fed into the electrode holder via a 4.7-MΩ resistor. From a computer-based analysis of the corresponding equivalent circuit the input capacitance, C_i, and the input resistance, R_i, of the system were determined to be 80 pF and >1 GΩ, respectively. From the corner frequency of the gain (determined by graphical evaluation) the same value for the input capacitance could be calculated according to:

$$f_c = 1/(2\pi RC), \qquad (4)$$

using $R = 4.7$ MΩ and $f_c = 420$ Hz.

Fig. 3 illustrates frequency spectra of the gain and the phase-shift for the whole electrical setup. In this experiment the two (geometrically nearly identical) source and potential-recording electrodes were placed in ASW and connected directly to the function generator and to the amplifier. The maximum gain was −40 dB, which means that the maximum voltage across the cell membrane was ~5 mV by an input signal ~0.5 V. Such a small potential was chosen to avoid nonlinear effects in
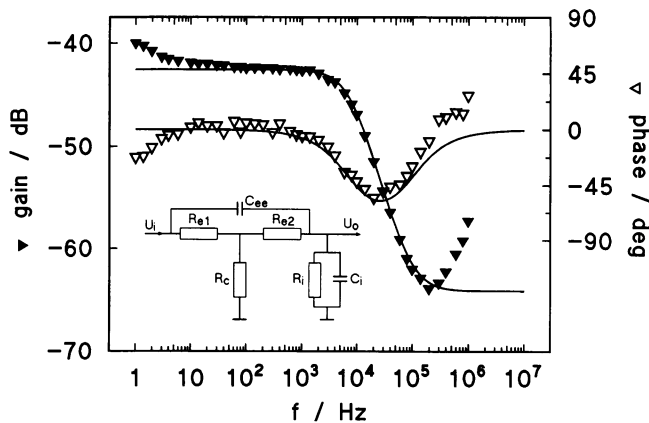
FIGURE 3 Typical frequency dependence of the gain and the phase-shift for the whole electrical setup (without the cell). In this experiment both microelectrodes were placed in ASW and connected directly to the function generator and to the amplifier. The reference electrode was connected through the resistance R_c (R_c = 10 kΩ) to ground. The curves were fitted by computer-based analysis of the frequency spectrum of the electronic circuit shown in the inset. *Inset,* Equivalent circuit for evaluation of the frequency spectrum of the whole electrical setup. R_{e1} and R_{e2}, resistances of the source and potential-measuring microelectrodes; C_{ee}, stray capacitance between the two microelectrodes; C_i and R_i, input capacitance and resistance of the amplifier, respectively (see text); and R_c = 10 kΩ.

the cell membrane (33). The frequency response can be simulated using the electronic circuit shown in the inset of Fig. 3. The deviation between the calculated (*solid lines*) and the experimentally determined curves (*open* and *filled triangles*) in the very low frequency range (1–10 Hz) resulted from polarization of the reference electrode. The analysis of the circuit of Fig. 3 (and of other circuits) demonstrated that the assumption of a stray capacitance, C_{ee}, between the two internal microelectrodes was essential for a satisfactory fit of the experimental data. This result was somewhat surprising since we had to assume a very small value (40 fF) for C_{ee} to obtain a reasonable fit to the data.

The resistance of the source electrode, R_{e1}, used in this specific experiment averaged 136 ± 13 kΩ (in ASW). It was not changed significantly by insertion into the cell or by the performance of several frequency runs (138 ± 12 kΩ in cells, evaluated from Fig. 4). After withdrawal of the source electrode from the cell, the same resistance was measured (139 ± 12 kΩ in ASW). In contrast, the electrode used to record the membrane potential showed an increased resistance, R_{e2}, after impaling the cell and several measurements of frequency spectra (from 208 ± 14 kΩ in ASW to 284 ± 17 kΩ in cells evaluated from Fig. 4). After withdrawal of the electrode from the cell the resistance was still slightly higher (227 ± 15 kΩ in ASW) than its initial value. The resistance, R_z, in the inset of Fig. 4 was calculated to be 134 ± 12 Ω. This resistance is determined by the conductivity of the cell interior, the conductivity of the external medium, and the resistance of the reference electrode.

It has to be noted that the evaluation of the transfer functions of the measurement apparatus was essential for the harmonic analysis of the electrical properties of *V. utricularis*. The reason for this is that the microelectrodes and the input capacitance of the amplifier made a substantial contribution to the transfer function that cannot be neglected when calculating the electrical properties of the cell. Furthermore, it was necessary to use equivalent circuits when fitting the Bode plots because the transfer functions reflect the response of the whole system, and not only that of the cell membrane impedance. Again the electrical properties of the cell have to be separated from those of the setup on the basis of equivalent circuits for the evaluation of the parameters of the transport.

Recording of gain and phase-shift at seven frequencies per decade was sufficient to obtain the frequency spectra with the required resolution (see above). Using this procedure, the time for the measurement of the total spectra could be reduced to <8 min. 0.5-V input voltage did not give a detectable output signal above 1 kHz. Therefore, the low frequency range (<1 kHz) was investigated with input voltages between 100 and 500 mV and the frequency range >1 kHz with input voltages of up to 1.4 V. It has to be noted that the voltage across the cell membrane was always <5 mV and that the exposure of cells to the field for 8 min did not cause substantial heating nor did it significantly disturb cell and membrane functions. In addition, repeated measurements of frequency spectra of the same cell (increasing the frequency up to 10 MHz followed by a decrease to 1 Hz) yielded identical
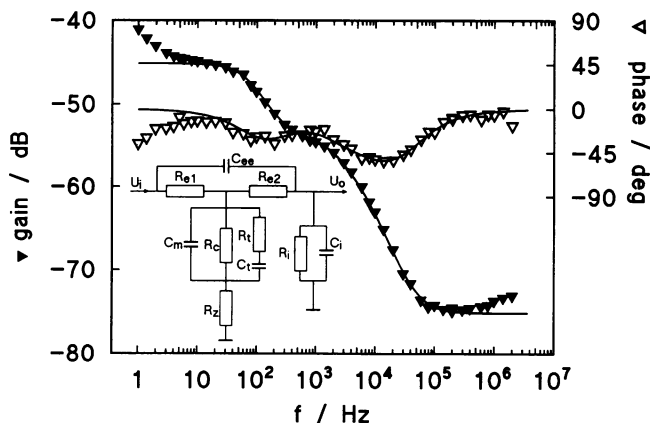

FIGURE 4 Typical frequency dependence of the gain and the phase-shift of a cell of *V. utricularis* placed in ASW (pH 8.1). The curves were fitted by computer-based analysis of the electronic circuit shown in the inset. Note that the presence of the Cl^--transport system leads to a characteristic change of the slope of the gain curve (and correspondingly of the phase-shift curve) in the 100 Hz to 10 kHz range. *Inset,* Equivalent circuit for interpretation of the frequency spectra. The symbols R_{e1}, R_{e2}, C_{ee}, C_i, and R_i have the same meaning as in Fig. 3. R_z, mixed resistance (related to the internal conductivity of the cell, the external conductivity of ASW, and to the resistance of the reference electrode). The symbols C_m, R_m, R_t, and C_t have the same meaning as in Fig. 2 *B*.

Cell	R_m^*	R_m	C_m	R_t	C_t	K_{AS}	K_S	N_0
	Ωcm^2	Ωcm^2	$\mu F/cm^2$	Ωcm^2	$\mu F/cm^2$	s^{-1}	s^{-1}	$pmol/cm^2$
1 (A)	1086	1005	0.69	201	3.78	549	110	5.70
2 (A)	961	809	0.58	302	2.98	404	151	5.89
3 (A)	1100	920	0.78	54	5.22	1676	98	6.13
4 (A)	848	694	0.48	231	1.82	894	297	3.39
5 (M)	1068	970	0.64	187	2.89	775	150	4.31
6 (M)	735	632	0.50	200	2.99	635	201	5.42
7 (M)	784	687	0.52	347	1.59	601	304	3.77
8 (M)	680	568	0.56	400	1.88	390	275	5.46
9 (M)	545	459	0.67	241	2.57	529	278	6.26

The experiments were performed in ASW (A) or MSW (M), pH 8.1; $T = 20°C$. The values of the passive electrical parameters of the membrane barrier and of the kinetic parameters of the Cl^--transport system were calculated from experimentally determined frequency spectra analogous to those shown in Fig. 4, by using the equivalent electric circuits in the inset of Fig. 4 (for curve fitting) and Fig. 2 A. R_m^* was determined by current-clamp.

gain and phase-shift curves within the limits of experimental resolution. Furthermore, determination of the membrane resistance by current-clamp measurements before and after (repeated) measurements of frequency spectra yielded cell membrane parameters, which were comparable with those obtained by harmonic system analysis (see Table 1).

Harmonic analysis of V. utricularis

Fig. 4 shows typical spectra of gain and phase-shift as derived from a V. utricularis cell bathed in ASW. It is obvious from Fig. 4 that the cell membrane did not behave as a simple RC circuit. The presence of the electrogenic chloride transport in the plasmalemma led to a change of the slope of the gain curve correlated with a change in the slope of the phase-shift between 100 Hz and 1 kHz. Bode plots of gain and phase-shift in Fig. 4 were fitted using the corresponding equivalent circuit given in the inset of Fig. 4 (solid lines in Fig. 4). The fit yielded values for R_m, C_m, R_t, and C_t, which were used for the calculation of the kinetic parameters of the chloride-carriers according to Eqs. A29–A41. The results for the cell of Fig. 4 were $N_0 = 3.39$ pmol/cm^2, $K_S = 297$ 1/s, and $K_{AS} = 894$ 1/s.

Table 1 contains the experimental results of nine cells together with the translocation rate constants, K_{AS} and K_S, of the complexed and the free form, respectively, and the total carrier concentration, N_0. The mean values for the parameters from the nine cells of Table 1 were $N_0 = 5.15 \pm 1.06$ pmol/cm^2, $K_S = 207 \pm 83$ 1/s, and $K_{AS} = 717 \pm 394$ 1/s. The real translocation rate constants, k_{AS} (=4700 1/s) and k_S (=256 1/s), could be calculated from K_{AS} and K_S by assuming $K = 0.3$ 1/M and $c = 599$ mM (see Appendix and reference 32). It has to be noted that the values of the specific capacitance and the specific resistance derived from the harmonic analysis were in the same range as those that have been obtained previously from charge pulse experiments (30, 31, 34). The variations in these two parameters from cell to cell were

quite normal. Current-clamp and harmonic analysis gave similar values for the specific resistance when measured on the same cell. Replacement of ASW by MSW did not lead to a significant change in the electrical parameters. The total surface concentration of carriers (N_0) and the translocation rates of the free (k_S) and the complexed form (k_{AS}) of the carriers were also in the same range as previously published (32).

We have shown in several studies that the surface concentration of "mobile" charges (i.e., the total surface density of charged carriers, N_{AS}) and the translocation rate, k, in the plasmalemma of V. utricularis are very sensitive to low pH (30, 31). To study this pH effect on the transfer function with harmonic analysis, we performed the following experiments. First, spectra of gain and phase-shift were taken from a cell at pH 8.1. (Triangles in Fig. 5. The data of phase-shift was not shown.) Subsequently the external pH was lowered to 4 (squares) and taken back to 8.1 (circles). The pH decrease to 4 resulted in the disappearance of the contribution of the carrier system to the Bode plot. The gain was much higher at pH 4 (as compared with pH 8) because the membrane resistance increased. The gain dropped linearly from the corner frequency at 30 Hz to the corner frequency at 10 kHz (see Fig. 5). When the pH was taken back to 8.1 these effects were not fully reversible even within 20 h, probably because the cell was exposed to pH 4 for too long, and because some of the carrier sites were inactivated (31). Lowering the external pH to 6 resulted only in an increase of the gain at low frequencies (<100 Hz, Fig. 6). However, in this case, the pH effect was fully reversible as Fig. 6 clearly demonstrates.

The effect of pH 4 and 6 on passive cell membrane properties and the kinetic parameters of carrier-mediated chloride transport are summarized in Table 2. The specific capacitance is the only parameter that was virtually pH independent. The specific resistance increased ≥ 10-fold at pH 4 and about 3- to 4-fold at pH 6, caused by a dramatic change of the carrier kinetics. At
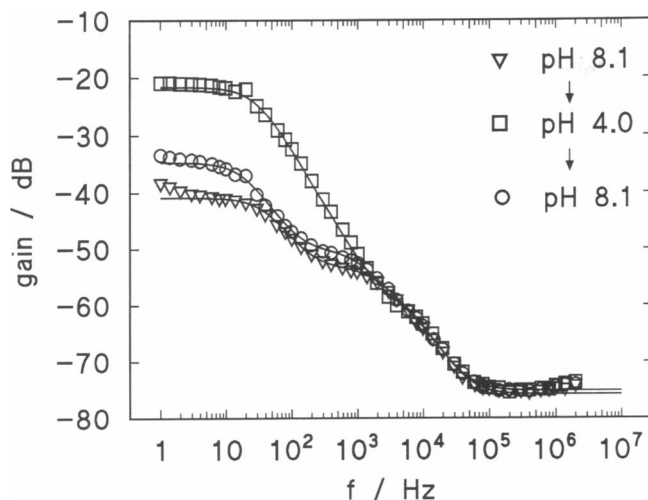
FIGURE 5 Frequency dependence of the gain of a *V. utricularis* cell at various pH values. Measurements were performed first at normal pH 8.1 (*triangles*), then 30 min after lowering of the pH to 4.0 (*squares*), and subsequently 1 h after reestablishment of the original pH value (*circles*). The curves were fitted by computer to the circuit in Fig. 4. Note that at pH 4.0 the electrical response of the Cl⁻-transport system has disappeared in the frequency range between 100 Hz and 10 kHz. Simultaneously, the membrane resistance was increased as indicated by the increase in the gain in the frequency range <100 Hz. For further discussion, see text.

pH 4 the cell membrane had only passive properties and it was impossible to calculate the rate constants and the surface density from the experimental data. The results at pH 6 show that the pH effect preferentially decreases the rate constant K_S.

DISCUSSION

Advantages and limitations of the harmonic analysis

There exist several different methods for the measurement of electrical properties of cell membranes. Some of these use microelectrodes inserted into a single cell and measure the electrical cell properties in a direct manner, such as the voltage-clamp and the charge-pulse techniques. These methods have a rather limited time resolution <10–100 kHz because of the membrane capacitance and the limitations of the measuring device (31, 35). Similarly, the frequency response of cell impedance measurements is limited to ~20 kHz (24). Harmonic analysis has the unique advantage of an extremely high frequency response that could be as high as 10 MHz. The disadvantage of the method is that the parameters cannot be related directly to the passive and active electrical properties of the cell membrane. Instead, an equivalent electrical circuit has to be used for the evaluation of membrane capacitance and resistance and the parameters of the electrogenic transport system. Furthermore, the electrical properties of the setup including microelec-

trodes have to be known before it is possible to calculate the parameters of the cell membrane.

Our investigation is a further demonstration that it is possible to modulate an electrogenic transport system with AC. The basic difference is that other methods use the application of oscillating fields to cell suspensions for the evaluation of its effect on the Na,K-ATPase (13, 14). In these investigations the movement of ions has been measured by tracer flux measurements. The data have been analyzed on the basis of three or four state models similar to ours (9–12, 14). The results show that K transport is stimulated at 1 kHz whereas the Na flux increases at 1 MHz, both in a very narrow strength of the oscillating electrical field (between 1.5 and 2.5 V/cm) (14), which may be explained by the assumption that the Na⁺,K⁺-ATPase acts as a channel-like enzyme and not as a carrier (15). The voltage-dependent step in these investigations is not completely clear, however, since direct voltage-clamp experiments on heart cells and *Xenopus* oocytes suggest that the electrogenic step of the Na⁺,K⁺-ATPase for Na⁺,Na⁺ exchange is in the kHz range and has a steep voltage dependence (36, 37).

The data presented here show that the method of harmonic analysis was not only a useful tool for the determination of the electrical properties of microelectrodes, but also for the evaluation of electrical properties of biological membranes, including those of electrogenic transport systems. This was demonstrated by the measurements of frequency spectra of gain and phase-shift on *V. utricularis* cells. Harmonic system analysis yielded membrane capacitance and resistance, and kinetic parameters of carrier-mediated chloride transport. This means that it was not necessary to know their properties a priori. It was
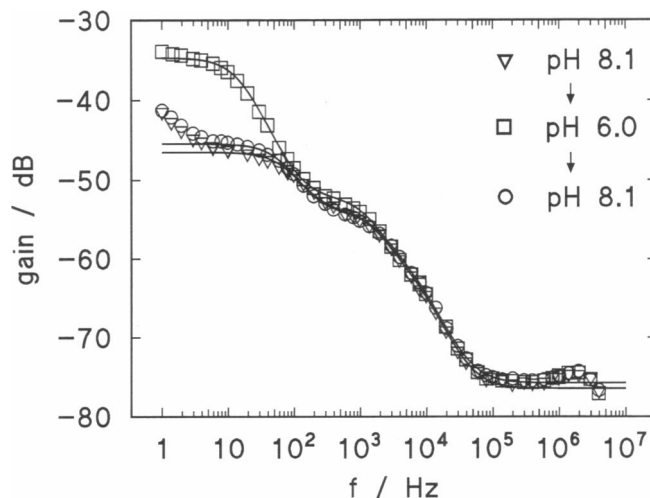

FIGURE 6 Analogous frequency spectra to those in Fig. 5 with the exception that the pH was lowered only to a value of 6.0. It is clear that at this pH a part of the transport system is still present. In contrast to Fig. 5 the pH effect on the transport system is completely reversible after reestablishment of the original pH of 8.1. The symbols have the same meanings as in Fig. 5.

pH	R_m^*	R_m	C_m	R_t	C_t	K_{AS}	K_S	N_0
	Ωcm^2	Ωcm^2	$\mu F/cm^2$	Ωcm^2	$\mu F/cm^2$	s^{-1}	s^{-1}	$pmol/cm^2$
Cell 5 (M)								
8.1	1,608	970	0.64	187	2.89	775	150	4.31
4.0	10,543	10,823	0.59	—	—	—	—	—
8.1	2,370	2,146	0.59	326	2.89	461	70	4.02
Cell 6 (M)								
8.1	736	632	0.50	200	2.99	635	201	5.42
4.0	18,806	18,040	0.50	—	—	—	—	—
8.1	2,209	1,904	0.50	160	4.29	670	57	5.28
Cell 7 (M)								
8.1	748	687	0.52	347	1.59	601	304	3.77
4.0	6,709	7,634	0.43	—	—	—	—	—
8.1	1,506	1,527	0.51	278	2.45	622	113	3.59
Cell 8 (M)								
8.1	680	568	0.56	400	1.88	390	275	5.72
6.0	1,763	1,679	0.56	280	4.00	383	64	5.71
8.1	573	480	0.56	200	2.38	837	498	4.40
Cell 9 (M)								
8.1	545	459	0.67	241	2.57	301	158	5.98
6.0	2,246	2,124	0.61	245	4.04	452	52	5.26
8.1	640	531	0.61	204	2.94	604	231	5.90

The experiments were performed in MSW, titrated to the indicated pH, and buffered either with 10 mM malic acid-NaOH (pH 4) or with 10 mM MES-NaOH (pH 6); $T = 20°C$. The experiments were performed as shown in Figs. 5 (pH 4) and 6 (pH 6). The values of the passive electrical parameters of the membrane barrier and of the kinetic parameters of the Cl⁻-transport system were calculated from experimentally determined frequency spectra analogous to that shown in Fig. 4, by using the equivalent electric circuits in the inset of Fig. 4 (for curve fitting) and Fig. 2 A. R_m^* was determined by current-clamp. Note that the algal cells show only passive properties at pH 4, i.e., the rate constants K_{AS} and K_S and N_0 could not be evaluated at that pH.

possible to design an electric equivalent circuit in accordance with the experimental results. From the electric circuit the passive and kinetic parameters of the cell membrane could be calculated. These parameters were similar to those that have been derived previously from charge-pulse experiments (32).

This agreement clearly indicated that the voltages applied to the cell membrane did not change its electrical properties. This was also not expected since the voltages imposed on the cell membrane during the harmonic analysis were on the order of 5 mV. It has to be noted that such effects could not be excluded a priori, if electrical rectification properties of the membrane barrier were taken into consideration. The good agreement of the results obtained by two different methods confirmed the model that was proposed earlier for carrier-mediated chloride transport (32).

Harmonic analysis of the carrier-mediated chloride transport

Besides the passive properties of the cell membrane, harmonic analysis also allows the evaluation of the parameters of carrier-mediated chloride transport. The results were in good agreement with those obtained earlier by two different methods and confirmed the postulated model (32, 35). The chloride transport of V. utricularis has some similarities with the chloride pump of Acetabularia (38–40). In particular, both transport systems have

similar surface densities of the carrier sites, and the voltage-independent steps involved in ion transport are rate limiting. We also could demonstrate that the external pH had a strong effect on chloride transport. Acidification to pH resulted in a successive disappearance of the contribution of the transport system to the Bode plots. This result was expected, since the "mobile" charges in the membrane of V. utricularis have been found to disappear in charge-pulse experiments at low pH (31). The interesting result of this study was that this disappearance had nothing to do with a titration of the negatively charged chloride-carrier complexes themselves. Instead, experimental results at pH 6 provided evidence that the translocation rate constant, K_S, of the free form decreased. Possibly, the carrier protein became immobilized when negative charges were protonated at low pH.

No contribution of the vacuole?

At pH 4 the spectra of gain and phase-shift were consistent with the passive properties of one single membrane. There was no indication that the large vacuole contributed to the electrical properties of the system. This result confirms that the tonoplast has a very low specific resistance, in agreement with our charge-pulse data (31, 32) and also with the results that have been derived from Valonia ventricosa (4), but contradicts the data of Davis (6). It has to be noted that the separation of the electrical properties of the tonoplast and the plasmalemma in
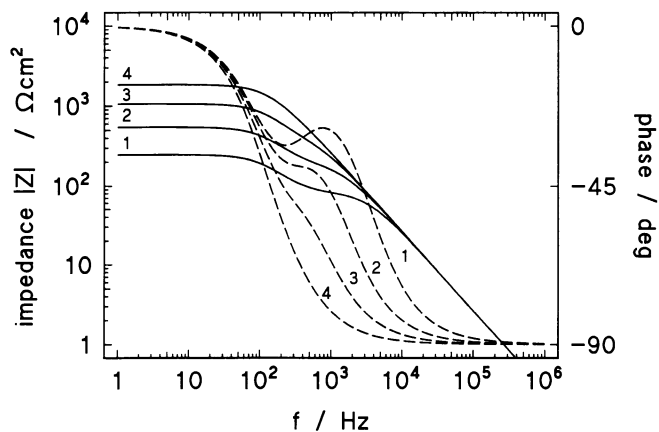
FIGURE 7 Influence of the surface concentration, N_0, of carrier sites on the Bode plots of the amplitude (*solid line*) and the phase-angle (*dotted line*) of impedance obtained from a computer simulation of the equivalent circuit given in Fig. 2 A. N_0 was decreased from 8 pmol/cm² (curve *1*) to 3 pmol/cm² (curve *2*), to 1 pmol/cm² (curve *3*), and to 0.1 pmol/cm² (curve *4*). The translocation constants of the free and complexed carriers, k_S and k_{AS}, were 410 and 4,600 1/s, respectively. The chloride concentration in the external ASW was set to 0.599 mM ($K = 0.3$ 1/M), $C_m = 0.6$ μF/cm², $R'_m = 2$ kΩcm², $T = 17°C$. Note that the dynamic properties of the membrane disappeared with decreasing concentration of carrier sites, N_0.

plant cells is very difficult since it is possible to insert the microelectrodes into the cytoplasm of the cell in only a very small number of cases (41).

Influence of the carrier system on gain and phase-shift: computer simulations of equivalent circuits

The results obtained from *V. utricularis* allows us to characterize the carrier system. This required variation of the different parameters of carrier-mediated chloride transport and evaluation of their influence on Bode plots. Fig. 7 demonstrates computer simulations of Bode plots of the amplitude (gain, *solid lines*) and the phase angle (phase-shift, *dotted lines*) of the membrane impedance according to the model in Fig. 2 A, as a function of the total concentration, N_0, of carrier sites. The highest surface concentration (8 pmol/cm²) was used for the simulation of the curves denoted by curve *1* ($k_S = 410$ 1/s, $k_{AS} = 4,500$ 1/s, $Kc = 0.18$, $C_m = 0.6$ μF/cm², and $R'_m = 2$ kΩ/cm²). Then N_0 was lowered to 3 pmol/cm² (curve *2*), to 1 pmol/cm² (curve *3*), and to 0.1 pmol/ cm² (curve *4*). The data of Fig. 7 show that the carrier system lost its influence on the gain (amplitude) and phase-shift when it was present at ~0.1 pmol/cm².

Further computer simulations showed that the relation between k_S and k_{AS} was essential for the observation of the characteristic effects of the transport system on Bode plots. Only for $k_{AS} > k_S$ did gain and phase-shift spectra allow the estimation of kinetic constants of carrier-mediated ion transport. For $k_S > k_{AS}$ the membrane system had only passive properties, although the pres-

ence of the carriers could increase the membrane conductance by many orders of magnitude. This is a general rule. Kinetic measurements of any type can be applied successfully only for kinetic analysis of carrier systems when the rate-limiting step is voltage independent (32, 42, 43).

The same conclusion can be derived from Fig. 8, which shows computer simulations of Bode plots as a function of k_{AS}. The curves for the amplitude and phase angle denoted by curve *1* were simulated using $k_{AS} = 4,500$ 1/s (the other parameters were the same as in Fig. 7). Then k_{AS} was decreased to 2,000 1/s (curve *2*), to 600 1/s (curve *3*), and to 200 1/s (curve *4*). In the latter case the influence of the transport system in the 0.1–10-kHz range disappeared, despite a high density of the carrier system. This means that a low surface density of the electrogenic transport system and/or a small translocation rate k_{AS} also may be the reason for the failure to detect transport systems within the membrane of other cells.

APPENDIX

Influence of a carrier system on the transfer functions

The mechanism of carrier-mediated transport has been described in detail in previous publications (32, 42, 44). The interested reader is referred to the review by Läuger et al. (45) for a complete description. In this publication we shall only list the basic assumptions of the model and the basic equations that are needed for the understanding of the harmonic analysis of carrier-mediated ion transport in the plasma-lemma of *V. utricularis*. Our model assumes a 1:1 carrier-ion complex that is formed at the membrane-solution interface. The heterogeneous complexation reaction is described by overall rate constants k_R (associa-
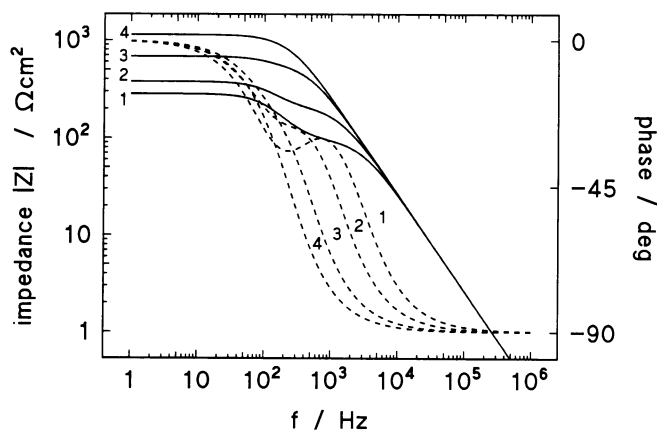

FIGURE 8 Influence of the translocation rate constant, k_{AS}, of the complexed carrier on the Bode plots of the amplitude (*solid line*) and the phase-angle (*dotted line*) of impedance obtained from a computer simulation of the equivalent circuit given in Fig. 2 A. k_{AS} was decreased from 4,500 1/s (curve *1*) to 2,000 1/s (curve *2*), to 600 1/s (curve *3*), and to 200 1/s (curve *4*). N_0 and k_S were set to 7 pmol/cm² and 400 1/s, respectively. All the other parameters were the same as in Fig. 7. Note that the dynamic properties of the membrane disappeared with decreasing translocation rate constant, k_{AS}.

tion) and k_D (dissociation). The stability constant of the carrier-anion complex is given by $K = k_R/k_D$. The translocation of the free and charged carriers, k_S and k_{AS}, respectively, are symmetrical and follow kinetics of simple first-order reactions. The translocation rate k_S is rate limiting and the translocation rate k_{AS} shows a voltage dependence of the Nernst–Planck-type (35, 43).

It is assumed that the membrane of *V. utricularis* separates identical solutions of chloride (concentration c) and that the carrier system is symmetrical. Denoting the interfacial concentrations of the free and complexed carriers on the left side of the membrane by N'_S and N'_{AS} and the concentrations on the right side by N''_S and N''_{AS} (expressed in mol/cm^2), then the change of these quantities with time is given by the following four differential equations:

$$\frac{dN'_{AS}}{dt} = (-k'_{AS}N'_{AS} + k''_{AS}N''_{AS}) + (-k_D N'_{AS} + k_R c N'_S), \quad (A1)$$

$$\frac{dN''_{AS}}{dt} = (k'_{AS}N'_{AS} - k''_{AS}N''_{AS}) + (-k_D N''_{AS} + k_R c N''_S), \quad (A2)$$

$$\frac{dN'_S}{dt} = (-k_S N'_S + k_S N''_S) + (k_D N'_{AS} - k_R c N'_S), \quad (A3)$$

$$\frac{dN''_S}{dt} = (k_S N'_S - k_S N''_S) + (k_D N''_{AS} - k_R c N''_S). \quad (A4)$$

It is assumed that the total surface concentration of carriers, N_0, complexed and free, is constant during an experiment:

$$N_0 = N'_{AS} + N''_{AS} + N'_S + N''_S = \text{const.} \quad (A5)$$

Of all the rate constants, only k'_{AS} and k''_{AS} are assumed to be voltage dependent. Their dependence may be calculated on the basis of a single barrier of the Eyring or Nernst–Planck type (43). For small voltages ($Vm \ll 25$ mV) the expressions may be linearized:

$$k'_{AS} = k_{AS}(1 + zu/2), \quad (A6)$$

$$k''_{AS} = k_{AS}(1 - zu/2). \quad (A7)$$

$u = FV_m/RT$ is the reduced voltage; V_m is the membrane voltage; F, R, and T have the usual meaning; and z is the valency of the carrier-ion complex.

The Cl$^-$-transport system in the plasmalemma of *V. utricularis* contributes not only to the membrane conductance but also has a considerable influence on the apparent membrane capacitance (31, 39). The total current density, $i_m(t)$, within the membrane has two parts:

$$i_m(t) = i_p + i_c. \quad (A8)$$

i_c is the current density caused by the movement of charged carriers within the membrane:

$$i_c = zF(k'_{AS}N'_{AS} - k''_{AS}N''_{AS}). \quad (A9)$$

i_p describes the current density due to the flux of ions through other transport pathways than the chloride carrier (conductance $1/R'_m$) and due to the capacitive current:

$$i_p = C_m dV_m/dt + V_m/R'_m. \quad (A10)$$

C_m is the membrane capacitance. The introduction of Eqs. A9 and A10 into Eq. A8 yields the following relation between current density and membrane voltage:

$$\frac{dV_m}{dt} = \frac{zF}{C_m}(-k'_{AS}N'_{AS} + k''_{AS}N''_{AS}) - \frac{V_m}{R'_m C_m} + \frac{i_m}{C_m}. \quad (A11)$$

Eqs. A1–A4 and Eq. A11 are a system of five coupled differential equations. The heterogeneous reaction between chloride and carrier is al-

ways in equilibrium for the chloride transport considered here. Accordingly, the five differential equations may be reduced to two as has been shown in Appendix A of Wang et al. (32):

$$\frac{du}{dt} = -\frac{8BN_0 K_{AS}}{z} v$$
$$-\left(\frac{1}{R'_m C_m} + 2BN_0 K_{AS}\right)u + \frac{F}{RTC_m}i_m, \quad (A12)$$

$$\frac{dv}{dt} = -2(K_S + K_{AS})v - \frac{zK_{AS}}{2}u, \quad (A13)$$

with the notations:

$$B = z^2 F^2/(4RTC_m), \quad (A14)$$

$$v = (N'_{AS} - N''_{AS})/(2N_{AS}), \quad (A15)$$

$$K_{AS} = \frac{Kc}{1 + Kc}k_{AS}, \quad (A16)$$

$$K_S = \frac{1}{1 + Kc}k_S. \quad (A17)$$

Laplace transformation transfers Eqs. A12 and A13 into a system of two linear equations for the complex variables $U(s)$ and $V(s)$, which are the Laplace transformations of $u(t)$ and $v(t)$, respectively. $I_m(s)$ is the Laplace transformation of $i_m(t)$.

$$sU(s) = -\frac{8BN_0 K_{AS}}{z}v(s)$$
$$-\left(\frac{1}{R'_m C_m} + 2BN_0 K_{AS}\right)U(s) + \frac{F}{RTC_m}I_m(s), \quad (A18)$$

$$sV(s) = -2(K_S + K_{AS})V(s) - \frac{zK_{AS}}{2}U(s). \quad (A19)$$

The replacement of $U(s)$ by $FU_m/(RT)$ in Eqs. A18 and A19 allows the calculation of the following equation for $U_m(s)$ (the Laplace transformation of Vm):

$$U_m(s) = G_m(s)I_m(s), \quad (A20)$$

with

$$G_m(s) = \frac{U_m(s)}{I_m(s)} = \frac{s + a}{C_m(s^2 + bs + c)}, \quad (A21)$$

with the notation

$$a = 2(K_S + K_{AS}), \quad (A22)$$

$$b = 2(K_S + K_{AS}) + 1/(R'_m C_m) + 2BN_0 K_{AS}, \quad (A23)$$

$$c = 2(K_S + K_{AS})(1/(R'_m C_m) + 2BN_0 K_{AS})$$
$$- 4BN_0 K_{AS}^2. \quad (A24)$$

$G_m(s)$ is the transfer function of the membrane-carrier system. The impedance of the cell membrane with the Cl$^-$-carrier $Z_m(i\omega) = G_m(i\omega)$ may be obtained by the replacement of the Laplace variable s by $i\omega$. This means that fitting the experimental membrane impedance data with the formalism described above allows the calculation of the parameters of carrier-mediated chloride transport, and of the passive membrane parameters.

The equivalent circuit of a membrane system has the same transfer function as the system itself. However, there may exist several equivalent circuits, which give a solution to this problem (i.e., which have the

same transfer function). One circuit is chosen that: (a) is composed of the smallest number of subunits and in which (b) all subunits have an appropriate biophysical meaning. The equivalent circuit A of Fig. 2 fulfills these conditions. It has the following transfer function:

$$G(s) = \frac{U(s)}{I(s)} = \frac{s + a}{C_m(s^2 + bs + c)}, \quad (A25)$$

with

$$a = 1/(R_1C) + 1/(R_2C), \quad (A26)$$

$$b = 1/(R_1C) + 1/(R_2C) + 1/(R'_mC_m) + 1/(R_1C_m), \quad (A27)$$

$$c = (1/(R_1C) + 1/(R_2C))(1/(R'_mC_m) + 1/(R_1C_m))$$
$$- (1/(R_1C_m)(1/(R_1C)). \quad (A28)$$

The comparison of the coefficients of Eq. A25 for $G(s)$ with those of Eq. A21 for $G_m(s)$ allows the derivation of the dynamic properties of the transport system from the properties of the equivalent circuit, i.e., the derivation of Eqs. A29–A34.

The following relations hold between the parameters, N_0, $K_{AS} = k_{AS}Kc/(1 + Kc)$ and $K_S = k_S/(1 + Kc)$ of the reaction model and the electric circuit A of Fig. 2:

$$N_0 = 2C/B_0, \quad (A29)$$

$$K_{AS} = 1/(2R_1C), \quad (A30)$$

$$K_S = 1/(2R_2C). \quad (A31)$$

C, R_1, and R_2 are given by the following relations:

$$C = B_0N_0/2, \quad (A32)$$

$$R_1 = 1/(B_0N_0K_{AS}) = 1/(B_0N_{AS}k_{AS}), \quad (A33)$$

$$R_2 = 1/(B_0N_0K_S) = 1/(B_0N_Sk_S), \quad (A34)$$

with

$$B_0 = (z^2F^2)/(2RT). \quad (A35)$$

The "apparent" capacitance, C, only depends on the carrier density, N_0, and increases linearly with increasing carrier density. The resistance, R_1, is proportional to the inverse of the translocation rate constant, k_{AS}, and the surface concentration, N_{AS}, of the charged carrier molecules. The resistance, R_2 is proportional to the inverse of the translocation rate constant, k_S, and to the surface concentration of the free carriers, N_S.

Between the elements of the circuits A and B shown in Fig. 2 the following relations hold:

$$R_t = (R_1 + R_2)/(R_1R_2), \quad (A36)$$

$$R_m = R_1 + R_2, \quad (A37)$$

$$C_t = C(R_2/(R_1 + R_2))^2, \quad (A38)$$

and

$$R_1 = R_tR_m/(R_t + R_m), \quad (A39)$$

$$R_2 = R_m^2/(R_t + R_m), \quad (A40)$$

$$C = C_t((R_t + R_m)/R_m)^2, \quad (A41)$$

with $R'_m \gg (R_1 + R_2)$. This means that the contribution of transport systems other than the chloride carriers to the membrane conductance is negligible compared with that of the electrogenic chloride transport. Both electric circuits, A and B of Fig. 2, were used for the analysis of the experimental data described in Results. The capacitance and resistance can be evaluated directly from the electric circuit B of Fig. 2, which

gave the optimal fit to the experimental data. After evaluation of the capacitances and resistances of the equivalent circuit A of Fig. 2 by using Eqs. A39–A41 the parameters of the carrier model could be calculated according to Eqs. A29–A31. This was done with this circuit because its components had a clearcut physical and/or biological meaning.

REFERENCES

1. Standen, N. B., P. T. A. Gray, and M. J. Whitaker. 1987. Microelectrode Techniques. Company of Biologists Limited, Cambridge, U.K.

2. Sakmann, B., and E. Neher. 1985. Single-channel Recording. Plenum Press, New York.

3. Arnold, W. M., and U. Zimmermann. 1988. Electrorotation: development of a technique for dielectric measurements on individual cells and particles. J. Electrostatics. 21:151–191.

4. Lainson, R., and C. P. Field. 1976. Electrical properties of Valonia ventricosa. J. Membr. Biol. 29:81–94.

5. Findlay, G. P., and A. B. Hope. 1976. Electrical properties of plant cells: methods and findings. In Encyclopedia of Plant Physiology. New Series. Transport in Plants II. U. Lüttge and M. G. Pitman, editors. Springer Verlag, New York. 53–92.

6. Davis, R. F. 1981. Electrical properties of the plasmalemma and tonoplast in Valonia ventricosa. Plant Physiol. (Bethesda). 67:825–831.

7. Beilby, M. J. 1989. Electrophysiology of giant algal cells. Methods Enzymol. 174:403–442.

8. Tsong, T. Y., and R. D. Astumian. 1988. Electroconformational coupling: how membrane-bound ATPase transduces energy from dynamic electric fields. Annu. Rev. Physiol. 50:273–290.

9. Robertson, B., and R. D. Astumian. 1990a. Kinetics of a multistate enzyme in a large oscillating field. Biophys. J. 57:689–696.

10. Robertson, B., and R. D. Astumian. 1991. Frequency dependence of catalyzed reactions in a weak oscillating field. J. Chem. Phys. 94:7414–7419.

11. Robertson, B., and R. D. Astumian. 1990b. Michaelis-Menten equation for an enzyme in an oscillating electric field. Biophys. J. 58:969–974.

12. Tsong, T. Y. 1992. Molecular recognition and processing of periodic signals in cells: study of activation of membrane ATPases by alternating electric fields. Biochim. Biophys. Acta. 1113:53–70.

13. Serpersu, E. H., and T. Y. Tsong. 1984. Activation of electrogenic Rb$^+$ transport of (Na,K)-ATPase by an electric field. J. Biol. Chem. 259:7155–7162.

14. Liu, D.-S., R. D. Astumian, and T. Y. Tsong. 1990. Activation of Na$^+$ and K$^+$ pumping modes of (Na,K)-ATPase by an oscillating electric field. J. Biol. Chem. 265:7260–7267.

15. Markin, V. S., D. Liu, J. Gimsa, R. Strobel, M. D. Rosenberg, and T. Y. Tsong. 1992. Ion channel enzyme in an oscillating electric field. J. Membr. Biol. 126:137–145.

16. Bode, H. W. 1945. Network Analysis and Feedback Amplifier Design. Van Nostrand, Reinhold, New York. Cole, K. S. 1972.

Membranes, Ions and Impulses. University of California Press, Berkeley, CA.

17. Aseltine, J. A. 1958. Transform Method in Linear System Analysis. McGraw-Hill Book Company, New York. Atherton, D. P. 1975. Non-Linear Control Engineering. Van Nostrand, Reinhold, New York.

18. Weiner, D. D., and J. F. Spina. 1980. Sinusoidal Analysis and Modeling of Weakly Non-linear Circuits. Van Nostrand, Reinhold, New York.

19. Schwan, H.-P. 1966. Alternating current electrode polarisation. Biophysik. 3:181–201.

20. Onaral, B., H. H. Sun, and H. P. Schwan. 1984. Electrical Properties of Bioelectrodes. IEEE (Inst. Electr. Electron. Eng.) Trans. Biomed. Eng. 31:827–832.

21. Moussavi, M., B. Onaral, Y. Y. Tsao, and H. P. Schwan. 1987. An automated instrument for high-precision interfacial impedance measurement in milli-Hz range. In Proceedings of the Thirteenth Annual Northeast Bioengineering Conference. K. R. Forster, editor. Publisher Institute of Electrical and Electronics Engineers, Inc., New York. 603–606.

22. Ragheb, T., and L. A. Geddes. 1990. Electrical properties of metallic electrodes. Med. Biol. Eng. & Comput. 28:182–186.

23. Hansen, U.-P., and D. Gradmann. 1971. The action of sinusoidally modulated light on the membrane potential of Acetabularia. Plant Cell Physiol. 12:335–348.

24. Tittor, J., U.-P. Hansen, and D. Gradmann. 1983. Impedance of the electrogenic Cl^- pump in Acetabularia: electrical frequency entrainements, voltage-sensitivity, and reaction kinetic interpretation. J. Membr. Biol. 75:129–139.

25. Tittor, J., U.-P. Hansen, and D. Gradmann. 1985. Spannungsabhängigkeit der Impedanz der elektrogenen Cl^--Pumpe von Acetabularia. Ber. D. Tsch. Bot. Ges. 98:143–154.

26. Correia, M. J., J. P. Landolt, M.-D. Ni, A. R. Eden, and J. L. Rae. 1981. A species comparison of linear and nonlinear transfer characteristics of primary afferents innervating the semicircular canal. In The Vestibular System: Function and Morphology. T. Gualtierotti, editor. Springer-Verlag, New York. 247–262.

27. Correia, M. J., B. N. Christensen, L. E. Moore, and D. G. Lang. 1989. Studies of solitary semicircular canal hair cells in the adults pigeon. I. Frequency- and time-domain analysis of active and passive membrane properties. J. Neurophysiol. 62:924–934.

28. Furman, J. M. R., T. C. Hain, and G. D. Paige. 1989. Central adaptation models of the vestibulo-ocular and optokinetic systems. Biol. Cybern. 61:255–264.

29. Sherman, K. R., E. L. Keller, and L. Stark. 1987. Simulations and sensitivity analysis of the vestibulo-ocular reflex. IEEE (Inst. Electr. Electron. Eng.) Trans. Biomed. Eng. 34:748–752.

30. Zimmermann, U., K.-H. Büchner, and R. Benz. 1982. Transport properties of mobile charges in algal membranes: influence of pH and turgor pressure. J. Membr. Biol. 67:183–197.

31. Benz, R., and U. Zimmerman. 1983. Evidence for the presence of mobile charges in the cell membrane of Valonia utricularis. Biophys. J. 43:13–26.

32. Wang, J., G. Wehner, R. Benz, and U. Zimmermann. 1991. Influence of external chloride concentration on the kinetics of mobile charges in cell membrane of Valonia utricularis. Evidence for the existence of a chloride carrier. Biophys. J. 59:235–248.

33. Astumian, R. D., and B. Robertson. 1989. Nonlinear effect of an oscillating electric field on membrane proteins. J. Chem. Phys. 91:4891–4901.

34. Walter, L., K.-H. Büchner, and U. Zimmerman. 1988. Effect of alkaline earth ions on the movement of mobile charges in Valonia utricularis. Biochim. Biophys. Acta. 939:1–7.

35. Wang, J., U. Zimmermann, and R. Benz. 1993. The voltage-dependent step of the chloride transporter of Valonia utricularis encounters a Nernst-Planck and not an Eyring type of potential energy barrier. Biophys. J. 64:1004–1016.

36. Nakao, M., and D. C. Gadsby. 1986. Voltage dependence of Na translocation by Na/K pump. Nature (Lond.). 323:628–630.

37. Rakowsky, R. F. 1992. Charge movement by Na/K pump in Xenopus oocytes. J. Gen. Physiol. 101:117–144.

38. Gerencser, G. A., J. F. White, D. Gradmann, and S. L. Bonting. 1988. Is there a Cl^- pump? Am. J. Physiol. 255:R677–R692.

39. Gradmann, D. 1975. Analog circuit of the Acetabularia membrane. J. Membr. Biol. 25:183–208.

40. Gradmann, D. 1989. ATP-Driven chloride pump in giant alga Acetabularia. Methods Enzymol. 174:490–504.

41. Bates, G. W., M. H. M. Goldsmith, and T. H. Goldsmith. 1982. Separation of tonoplast and plasma membrane potential and resistance in cells of oat coleoptiles. J. Membr. Biol. 66:15–23.

42. Benz, R., and P. Läuger. 1976. Kinetic analysis of carrier-mediated ion transport by the charge pulse technique. J. Membr. Biol. 27:171–191.

43. Benz, R., and S. McLaughlin. 1983. The molecular mechanism of action of the proton ionophore FCCP (carbonylcyanide p-trifluoromethoxyphenyl-hydrazone). Biophys. J. 41:381–398.

44. Läuger, P. 1972. Carrier-mediated ion transport. Science (Wash. DC). 178:24–30.

45. Läuger, P., R. Benz, G. Stark, E. Bamberg, P. C. Jordan, A. Fahr, and W. Brock. 1981. Relaxation studies of ion transport systems in lipid bilayer membranes. Q. Rev. Biophys. 14:513–598.